Effect of heat treatment on corrosion resistance of Al₂O₃-TiO₂ ceramic coating impregnated with aluminum phosphate

Tuan Nguyen Van[1*], Tuan Anh Nguyen[1], Ha Pham Thi[1], Ly Pham Thi[1], Phuong Nguyen Thi[1], Quy Le Thu[2]

[1]Institute for Tropical Technology, Vietnam Academy of Science and Technology, 18 Hoang Quoc Viet, Cau Giay, Ha Noi, Viet Nam

[2]National Key Laboratory for Welding and Surface Treatment Technologies, National Research Institute of Mechanical Engineering, 4 Pham Van Dong, Cau Giay, Ha Noi, Viet Nam

[*]Email: *nvtuan@itt.vast.vn*

Abstract. The atmospheric plasma spray process (APS) is a well-established and widely employed technology used to create various types of coating for the fabrication of numerous industrial applications. Speciallity, this process is considered as a suitable technique for fabricating ceramic coatings. However, the structure of thermal spray coatings consists of particles, semi-molten particles, oxides, pores, and cracks that significantly influence the coating properties, especially their erosion-corrosion resistance. In this study, the Al_2O_3-$40TiO_2$ coating applied by APS was penetrated with aluminum phosphate (APP) by ultrasonic excitation method, and then, the effect of heat treatment after the sealing on corrosion protection of Al_2O_3-$40TiO_2$ ceramic coating was investigated. The results show that, after being impregnated with APP, the heat treatment at 800 °C assures the coating a lower porosity and better corrosion resistance than heat treatments at 400 and 600 °C. The existence of the durable crystalline phases $Al(PO_3)_3$ (Cubic), $Al_2P_6O_{18}$ (Monoclinic), and $AlPO_4$ (Orthorhombic) on the surface of the sample heat-treated at 800 °C has contributed to enhancing the corrosion resistance of the Al_2O_3-$40TiO_2$ coating.

Keywords: Al_2O_3-$40TiO_2$ coating, erosion-corrosion, aluminum phosphate, heat treatment.

Classification numbers: 2.9.2, 2.9.4.

1. INTRODUCTION

It has been reported that sprayed Al_2O_3-TiO_2 composite ceramic coatings have high durability in various environments, especially in terms of corrosion and wear resistance [1, 2]. The corrosion resistance of Al_2O_3-TiO_2 coatings fabricated by the thermal spray-coating technique using combustible gas has been investigated by Pinzón *et al.* [3]. The results reveal that as the coating's porosity rises, its corrosion resistance effectiveness declines. The corrosion and wear resistance of Al_2O_3-13 wt.% TiO_2 composite ceramic coatings with nanostructures of

different porosity were studied by Tian *et al*. [4]. The authors indicated that the coating has low porosity, decent corrosion, and wear resistance in environments with high temperatures and pressure. The corrosion resistance of Al_2O_3-TiO_2 coating was investigated by Zavareh *et al*. [5]. According to the authors, the coating created by the APS method has better anti-corrosion ability than the coating created by the HVOF method. In 2010, the wear resistance of Al_2O_3-13wt.% TiO_2 and Al_2O_3-43wt.% TiO_2 composite ceramic coatings were investigated by Vargas *et al*. [6], the authors indicated that the Al_2O_3-13wt.% TiO_2 coating has higher wear resistance than the Al_2O_3-43wt.% TiO_2 coating. However, the corrosion resistance of Al_2O_3-43 wt.% TiO_2 coating is significantly higher than that of Al_2O_3-13wt.% TiO_2 coating. The nanographene with different structures (Gpt and GNs) has dramatically improved the wear resistance of Al_2O_3-13wt.% TiO_2 created by APS, which was investigated by Wang *et al*. [7]. The graphene nanoplatelets (GNPs) used to reinforce the Al_2O_3-40TiO_2 coating created by the APS method were investigated by Verma *et al*. [8]. According to the authors, the porosity of the coating decreased from 17 % to 6 % when the coating material was added with 1.5 % GNPs.

Many studies have shown that aluminum phosphate (APP) is highly effective in improving the corrosion resistance property of ceramic coatings and composite ceramic coatings [9 - 12]. In our previous works [13 - 16], the combination of sealing with APP and heat treatment for thermal coatings was also mentioned. The obtained experimental results demonstrated that after applying the treated method, the thermal spray coatings have excellent resistance to corrosion and wear corrosion. For example, when NiCr electric arc sprayed coating was impregnated with APP and heat-treated in the range of 400 to 1000 $^{\circ}$C, its corrosion resistance was enhanced considerably in comparison with the unsealed coating. After 1052 hours of immersion in pH 2.0 H_2SO_4 solution, for the unsealed samples, the boundary between the NiCr layer and the steel substrate had a clear separation, while for the sealed ones, this separation was insignificant and decreased with the higher the annealing temperature.

In addition, in the presence of ultrasonic excitation, APP had penetrated deeply into the coating through cracks, and open pores of the coating, thus the reducing porosity and the anti-corrosion protection of the coating were greatly enhanced [17, 18]. The ultrasonic waves accelerate thermal motion, reduce interfacial tension, and improve the compatibility between the coating and the penetrant. With the energy of ultrasonic waves, the air in the pores of the coating is pushed out, enabling APP to penetrate deeply into the pores. Moreover, the ultrasonic wave also causes the air contained in the APP to continuously escape by buoyancy force and pressure. This process is constantly repeated, through which a large amount of the penetrant is penetrated deeply into the coating. In this study, we carried out a penetration treatment for the coating with APP in the presence of ultrasonic excitation. The Al_2O_3-40TiO_2 coating after spraying was immersed in an ultrasonic vibration tank containing APP. Then, the coating is heat-treated in a temperature range of 400 to 800 $^{\circ}$C. The effect of the heat treatment on the erosion-corrosion resistance was investigated.

2. MATERIALS AND METHODS

2.1. Material preparation

The material of the substrate is carbon steel of dimension $50 \times 50 \times 3$ mm^3 with chemical composition listed in Table 1. The bond coat and top coat are fabricated from Ni20Cr and Al_2O_3-40TiO_2 powder, respectively. These powders have a particle size of 45 ± 5 μm, which is provided by Sulzer Metco. Table 2 is the detailed composition of the spray powders.

Table 1. Chemical composition of the carbon steel substrate.

Element	C	Si	Mn	P	S	Cr	Fe
Chemical composition, %	0.465	0.258	0.656	0.022	0.025	0.355	Bal.

Table 2. Chemical composition of the spray powders (wt.%).

Powder	Ni	Cr	Fe	Mn	Al$_2$O$_3$	TiO$_2$	Fe$_2$O$_3$	MgO	CaO	Other (max)
Ni20Cr	Bal.	19.5	1.0	1.5	-	-	-	-	-	≤ 1.7
Al$_2$O$_3$-40TiO$_2$	-	-	-	-	Bal.	39.5	≤ 0.3	≤ 0.2	≤ 0.1	

2.2. Coating fabrication and aluminum phosphate preparation

2.2.1. Coating fabrication

Before the spraying, the surfaces of the substrate were roughened by the α-Al$_2$O$_3$ abrasive blasting method with the parameters as follows: α-Al$_2$O$_3$ grain size of 0.8 ÷ 1.2 mm, grit blasting distance of 120 mm, blasting angle of 90°, and blasting pressure of 6 bar. Then, the sample's surface was cleaned with dry air before coating deposition. The coating application was performed on a PRAXAIR-TAFA plasma-spraying machine using the SG-100 spray gun with the technical parameters as shown in Table 3. The bond coat is NiCr20 with a thickness of about 100 μm and the thickness of the Al$_2$O$_3$-40TiO$_2$ coating is about 300 μm.

Table 3. Plasma-spraying operating parameters.

Spray Parameters	Ni20Cr bond	Al$_2$O$_3$-40TiO$_2$ coating
Spray angle	90°	90°
Spray distance, mm	120	100
Powder feed rate, g/min	20	30
Plasma current, A	550	600
Primary gas Ar, L/min	65	45
Secondary gas H$_2$, L/min	5	12
Nozzle moving speed, mm/min	~ 250 - 300	80 - 90

2.2.2. Aluminum phosphate preparation

Aluminum phosphate solution (APP) was prepared from the phosphoric acid solution (85 % H$_3$PO$_4$) and aluminum hydroxide powder Al(OH)$_3$ with a P/Al molar ratio of 3. After completion of the chemical reaction, the mixture was diluted with about 20 wt.% of deionized water and stirred until the solution became transparent. The aluminum phosphate was stored in solution at the ambiance for 12 hours.

2.2.3. Impregnation for the coating

The coating samples were immersed into APP in the presence of ultrasonic vibration for 5 hours with a vibration frequency of 30 kHz. After immersing, the samples were heat-treated at three temperature levels of 400 ^{o}C, 600 ^{o}C, and 800 ^{o}C for 2 hours and left to cool down in the oven for 12 hours [17]. After heat treatment, remove any remaining APP on the surface before analyzing the coating's properties.
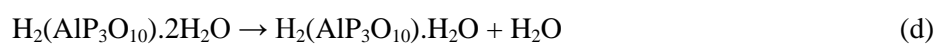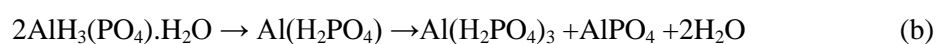
2.3. Characterization methods

The microstructure of the coatings was studied using a scanning electron microscope SM-6510LV (Japan). The anti-corrosion property of the coating was determined by electrochemical measurements: Dynamic potential curve scanning and electrochemical impedance spectroscopy (EIS) in 3.5 % NaCl solution. The polarization curve was scanned in a potential range from -250 to 250 mV around the open circuit potential (E_{ocp}). The polarization curves were obtained at a scan rate of 1 mV/s. The EIS curves of the coating samples were measured with oscillation amplitude $\Delta E = 5$ mV in the frequency range from 10^5 to 10^{-2} Hz, 7 points/decade. The Biologic VSP-300 electrochemical measuring instrument coupled with EClab software was used to study the anti-corrosion/corrosion properties of the coating. The phase composition of the residual aluminum phosphate on the coating surface was investigated by X-ray diffraction (XRD D5005/ SIEMENS) at 25 ^{o}C with Cu-Kα radiation, 2θ angle scanning from 10° to 70 ^{o}, a step width of 0.03^o [16, 19]. The erosion-corrosion resistance of the sample was tested by centrifugal spinning method, rotation speed 1000 rpm, corrosion test time 168 hours, in 3.5 % NaCl solution containing 0.25 % SiO_2 particles causing erosion. The change in the coating's appearance was observed with time during the erosion-corrosion test.

3. RESULTS AND DISCUSSION

3.1. Phase analysis

According to the literature, the phase composition of APP coating samples changes when the temperature increases. When heat-treated in the range of 60 - 80 ^{o}C, free water in the APP evaporates, resulting in $Al(H_2PO_4)_3.3H_2O$. When the treatment temperature is increased to 400 ^{o}C, $Al(H_2PO_4)_3.3H_2O$ salt turns into crystalline phases $[Al(PO_3)_3]_n$ (dominant phase) and $AlH_2P_3O_{10}.2,5H_2O$ (secondary phase). These phases will continue transferring to $Al_2P_6O_{18}$ and $Al(PO_3)_3$(cubic) when the temperature is in the range of 400 ^{o}C - 700 ^{o}C. When the temperature reaches 800 ^{o}C, besides the main phase of $Al(PO_3)_3$ (cubic), there is the formation of $AlPO_4$ (trigonal) [20, 21].

The water molecule separates from the APP compound according to the following chemical reactions from (a) to (f) [18].

$$AlH_3(PO_4)_2.3H_2O \rightarrow AlH_3(PO_4)_2.H_2O+H_2O \qquad (a)$$

$$2AlH_3(PO_4).H_2O \rightarrow Al(H_2PO_4) \rightarrow Al(H_2PO_4)_3 +AlPO_4 +2H_2O \qquad (b)$$

$$Al(H_2PO_4)_3 \rightarrow H_2(AlP_3O_{10}).2H_2O \qquad (c)$$

$$H_2(AlP_3O_{10}).2H_2O \rightarrow H_2(AlP_3O_{10}).H_2O + H_2O \qquad (d)$$

$$2H_2(AlP_3O_{10}).2H_2O \rightarrow Al_2P_6O_{18} +4H_2O \qquad (e)$$

$$Al_2P_6O_{18} \rightarrow 2Al(PO_3)_3 \qquad (f)$$

Although the heat treatment can reduce the porosity of the coating, the separation of water molecules from aluminum phosphate compounds during this process can affect the porosity treatment efficiency of APP due to the volume decreasing of APP solution in the pores.

In this research, the APP compound that remained on the coating surface after heat treatment was separated from the coating and then determined the phase composition by the XRD method (Figure 1). This is also the reason why the XRD patterns do not include the high intensity of peaks belonging to the steel substrate and the Al_2O_3-40TiO_2 coating.
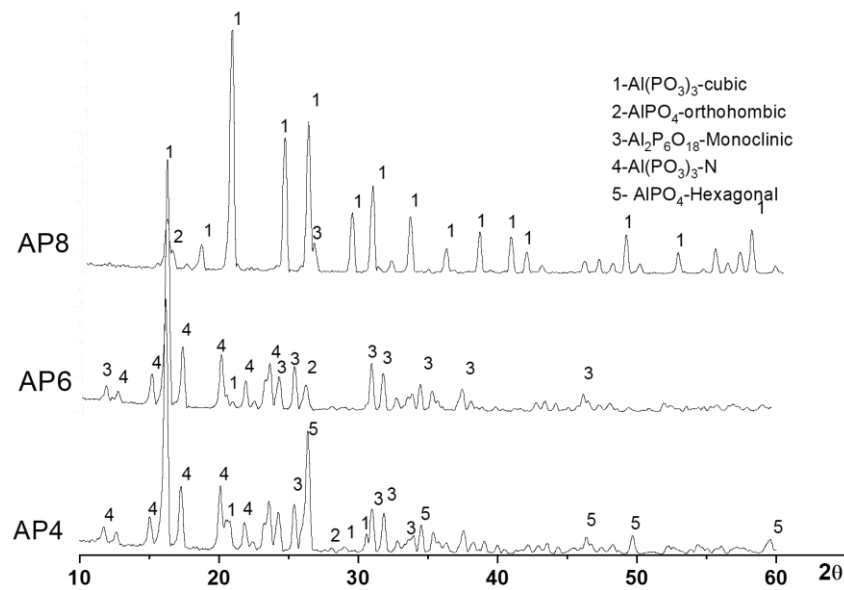
Figure 1. XRD spectra of coating samples.
(AP4 - The APP heat-treated at 400°C; AP6 - The APP heat-treated at 600 $^{\circ}$C;
AP8 - The APP heat-treated at 800 $^{\circ}$C).

On the XRD patterns of the AP4 sample, there are major crystalline phases of Al(PO$_3$)$_3$ (cubic), AlPO$_4$ (hexagonal), Al$_2$P$_6$O$_{18}$ (monoclinic), and Al(PO$_3$)$_3$ (N). However, on the XRD pattern of the AP6 sample, AlPO$_4$ (hexagonal) crystals were not found. The reason is that AlPO$_4$ (hexagonal) crystalline phase has changed to AlPO$_4$ (orthorhombic) in the increasing temperature process from 400 $^{\circ}$C to 600 $^{\circ}$C. Crystalline phases Al(PO$_3$)$_3$ (cubic), Al$_2$P$_6$O$_{18}$ (monoclinic), and AlPO$_4$ (orthorhombic), which are stable, were also found on the XRD pattern of the AP8 sample.

Moreover, in the XRD result, no new compound consisting of the original coating elements was detected. This can indicate that the sealing mechanism of APP is only adhesive bonding.

3.2. Cross-sectional structure of the coating

Figure 2 shows the cross-sectional images of the Al$_2$O$_3$-40TiO$_2$ coating taken by a scanning electron microscope. It can be seen that the coating has a heterogeneous structure. However, the structure tends to become more uniform after sealing with APP and being heat treated at 400 and 800 $^{\circ}$C. After heat treatment at 800 $^{\circ}$C, the coating had less porosity than those treated at 400 $^{\circ}$C and 600 $^{\circ}$C. The reason might be that besides the porosity treatment efficiency of APP, the thermal diffusion also took place strongly at 800 $^{\circ}$C. Conversely, the PR6 sample had the highest porosity and cracks in comparison with other treated ones due to the separation of water molecules from aluminum phosphate compound AlH$_2$P$_3$O$_{10}$.2,5H$_2$O (the secondary APP phase at 400 $^{\circ}$C) during the process of increasing temperature from 400 $^{\circ}$C to 600 $^{\circ}$C [20]. After being separated from the aluminum phosphate, the vaporized water escapes from the coating causing many small cracks and pores in the RP6 coating's structure. In the XRD patterns (Figure 1), AlH$_2$P$_3$O$_{10}$.2,5H$_2$O did not appear because its content seems to be low.
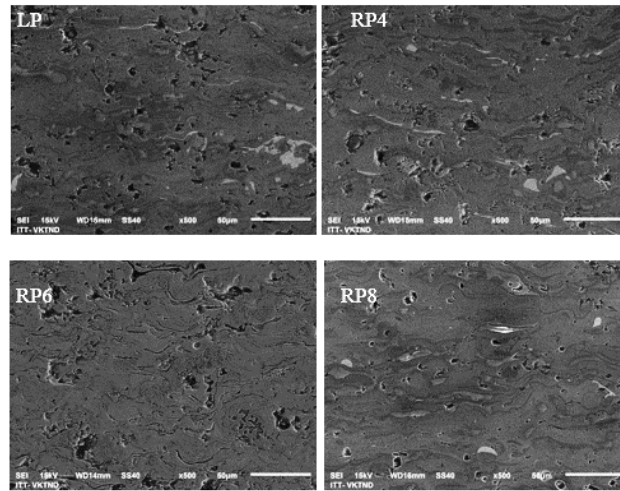
Figure 2. SEM cross-sectional image of the Al_2O_3-40TiO_2 coating (×500).

(LP - Coating without APP permeation treatment; RP4 - Coating permeation-treated with APP in the presence of ultrasonic excitation and heat-treated at 400 ^{o}C; RP6 - Coating permeation-treated with APP in the presence of ultrasonic excitation and heat-treated at 600 ^{o}C; RP8 - Coating permeation-treated with APP in the presence of ultrasonic excitation and heat-treated at 800 ^{o}C).

3.3. Potentiodynamic polarization

The corrosion resistance property of the coating was investigated by scanning the dynamic potential polarization curve in the 3.5 % NaCl solution (Figure 3). In which, the cathodic polarization branch is related to the reduction of dissolved oxygen and the anodic polarization branch corresponds to the anti-corrosion of the coating [22, 23]. E_{corr} is the corrosion potential of the coating, which depends on the electrochemical reaction between the anode and the cathode. Besides the corrosion potential, corrosion current density (i_{corr}) is also an essential parameter that represents the corrosion resistance of the coating. A more positive value of the corrosion potential or a smaller current density indicates that the coating has greater corrosion resistance [22].

The corrosion potential (E_{corr}) values and the corrosion current density (i_{corr}) obtained from these curves by Tafel fitting using EClab software are listed in Table 4. Electrochemical parameters E_{corr} and I_{corr} of the samples were determined according to the expression of Stern–Geary (1) [24].

$$i_{corr} = \frac{\beta a x \beta c}{2.303 \, (\beta a + \beta c) x Rp} = \frac{B}{R_p} \tag{1}$$

as shown in Figure 3, E_{corr} of RP4 and RP8 samples shifted more to the positive side than E_{corr} of the LP sample. Meanwhile, E_{corr} of the RP6 sample shifted more to the negative side than E_{corr} of the LP sample. The corrosion potential of RP6 was the lowest among corrosion potential values of the treated samples with APP because of the largest number of pores and cracks in its structure. During the process of increasing temperature from 400 ^{o}C to 600 ^{o}C, the aluminum phosphate compound $AlH_2P_3O_{10}.2,5H_2O$ (the secondary phase of aluminum phosphate at 400 ^{o}C) was dehydrated [20, 21]. The water evaporation from the aluminum phosphate is the root of creating many small cracks and pores in the coating's structure. These cracks contribute to

468

promoting corrosion in the RP6 coating. Moreover, the corrosion current density values of three treated samples with APP listed in Table 4 also have the same sort order as the corrosion potential.

In comparison between the RP6 sample and LP sample, E$_{corr}$ of the RP6 sample shifted more to the negative side than E$_{corr}$ of the LP sample, but the corrosion current density the of RP6 sample (i$_{corr}$ ≈ 4.907 µA/cm^2) is significantly smaller than that of the LP sample (i$_{corr}$ ≈ 24.608 µA/cm^2). This indicates that the coating impregnated with aluminum phosphate and heated treatment has higher corrosion resistance than the untreated coating with aluminum phosphate. This proves that the sealing APP and heat treatment improved the corrosion resistance of the RP4, RP6, and RP8 samples.
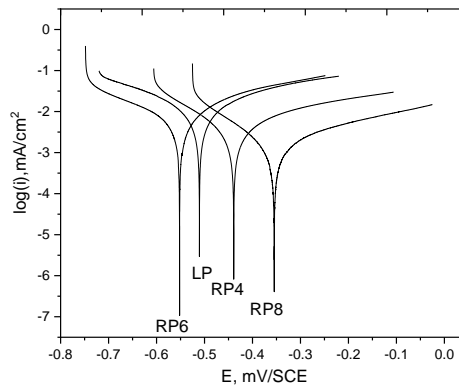

Figure 3. Polarization curves of different coating samples in 3.5 wt.% NaCl solution.
(LP – Coating without APP permeation treatment; RP4 – Coating permeation-treated with APP in the presence of ultrasonic excitation and heat-treated at 400 $^{\circ}$C; RP6 – Coating permeation-treated with APP in the presence of ultrasonic excitation and heat-treated at 600 $^{\circ}$C; RP8 – Coating permeation-treated with APP in the presence of ultrasonic excitation and heat-treated at 800 $^{\circ}$C).

Table 4. Determined corrosion parameters from polarization curves measured in 3.5 % NaCl solution.

Samples	E$_{corr}$	i$_{corr}$	R$_p$	S$_i$
LP	- 518.678	24.608	1.542	-
RP4	-438.666	2.647	9.855	89.24
RP6	-551.766	4.907	5.316	80.05
RP8	-353.786	1.159	22.505	95.29

In Table 4, the porosity treatment efficiency (S$_i$) of the sealed coatings which is calculated according to expression (2) is also recorded. Whereby, the porosity treatment efficiency of the RP4, RP6, and RP8 samples are 89.24 %, 80.05 %, and 95.29 %, respectively. These values demonstrate that the coating permeation-treated with APP and heat treated at 800 $^{\circ}$C has the lowest porosity in comparison with the sealed others. The LP sample was not treated with aluminum phosphate, so it has no porosity treatment efficiency.

$$S_i = \frac{I_{corr}}{I_C} \times 100 \text{ \% [12]} \tag{2}$$

in which: I$_C$ is the corrosion current density of untreated coating with APP; I$_{corr}$ is the corrosion current density of treated coatings with aluminum phosphate.

The EIS method could be used to determine the mechanism of electrochemical processes occurring on the interface [25]. For our samples, the Nyquist impedance plot is shown in Figure 4a and the Bode impedance plot is shown in Figure 4b. Equivalent circuit diagram $R+Q_1/(R_1+Q_2/R_2)$ was selected to simulate the corrosion behavior of Al_2O_3-40TiO_2 coating in 3.5 % NaCl solution. In which, R is the resistance of the solution. R_1 is the resistance to current flow through the pores in the coating and R_2 indicates the charge transfer resistance [12]. R_1 and R_2 depend on the ion exchange process in the pores of the coating and the corrosion process that occurs for the steel substrate. Q_1 and Q_2 are phase constants that characterize the diffusion process in the pores of the coating and on the interface between the coating and the steel substrate [22, 26]. The R and Q values shown in Table 5 were obtained from the electrochemical impedance spectroscopy analysis using EClab software.

$$Z = \frac{1}{Q_1(i2\pi f)^{\alpha 1}} \ [27] \tag{3}$$

as can be seen in Table 5, the samples impregnated with APP and heat-treated have higher corrosion resistance than the untreated coating samples. In addition, for the samples penetration-treated with APP in the presence of ultrasonic excitation and heat treatment, the highest R_2 value of the RP8 sample demonstrates the best corrosion protection of the sample heat-treated at 800 ^{o}C. In contrast, after heat treatment at 600 ^{o}C, the sample has the lowest R_2 value, indicating that its corrosion resistance is the worst. The reason is that R_2 indicates the charge transfer resistance at the interface between the coating and the steel substrate. This value characterizes the anti-corrosion protection ability of the coating for the substrate. The R_2 values of the samples are different due to the difference in the porosity and number of cracks in the structure of the coatings which is explained in section 3.2.

Table 5. Electrochemical parameters determined from the equivalent circuit diagram.

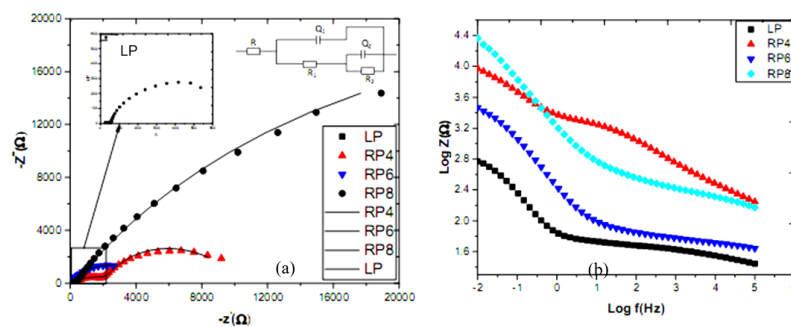| Samples	R (Ω)	Q_1(F.s$^{(\alpha-1)}$)	R_1 (Ω)	α_1	Q_2 (F.s$^{(\alpha-1)}$)	R_2 (kΩ)	α_2
LP	41.96	0.001389	68.45	0.1879	0.005153	1673	0.5805
RP4	86.34	0.00005199	2770	0.4412	0.000308	7895	0.8197
RP6	29.27	0.0002795	42.77	0.7526	0.0008553	5552	0.7526
RP8	95.48	0.00003449	256.2	0.4559	0.0001605	69242	0.5003

Figure 4. Nyquist plots (a) and Bode plots (b) of the coating samples.
LP - Coating without APP permeation treatment; RP4 - Coating permeation-treated with APP in the presence of ultrasonic excitation and heat-treated at 400 ^{o}C; RP6 - Coating permeation-treated with APP in the presence of ultrasonic excitation and heat-treated at 600 ^{o}C; RP8 - Coating permeation-treated with APP in the presence of ultrasonic excitation and heat-treated at 800 ^{o}C.

In the Bode plot (Figure 4b), the low-frequency region characterizes the corrosion process of the steel substrate and the high-frequency region characterizes the electrochemical process in the coating [12]. Research results show that |Z| measured in the low-frequency region for sample RP8 is larger than that of other coating samples, this result further confirms that RP8 sample has greater corrosion resistance than RP4 and RP6 samples.

3.4. Erosion-corrosion test

The results of the erosion-corrosion test for 168 hours are shown in Figure 5. It shows that the appearing red rust spots were observed on the surface of the LP and RP6 samples after 24 hours of the test as well as on the surface of the RP4 sample after 168 hours. Meanwhile, the rust phenomena have not occurred in the RP8 sample during the testing process. The result proves that the erosion/corrosion resistance of the samples in NaCl solution containing the causative agent of erosion in descending order are as follows RP8, RP4, and RP6. RP6 is the worst, almost like the untreated sample LP while the sample with lower treated temperature RP4 is better. This is also consistent with the above research result about the structure of the samples. As explained in section 3.2, after heat treatment at 600 ^{o}C, the water molecules in the aluminum phosphate were separated and evaporated causing small cracks and pores in the coating reducing the erosion - corrosion resistance of the coating.
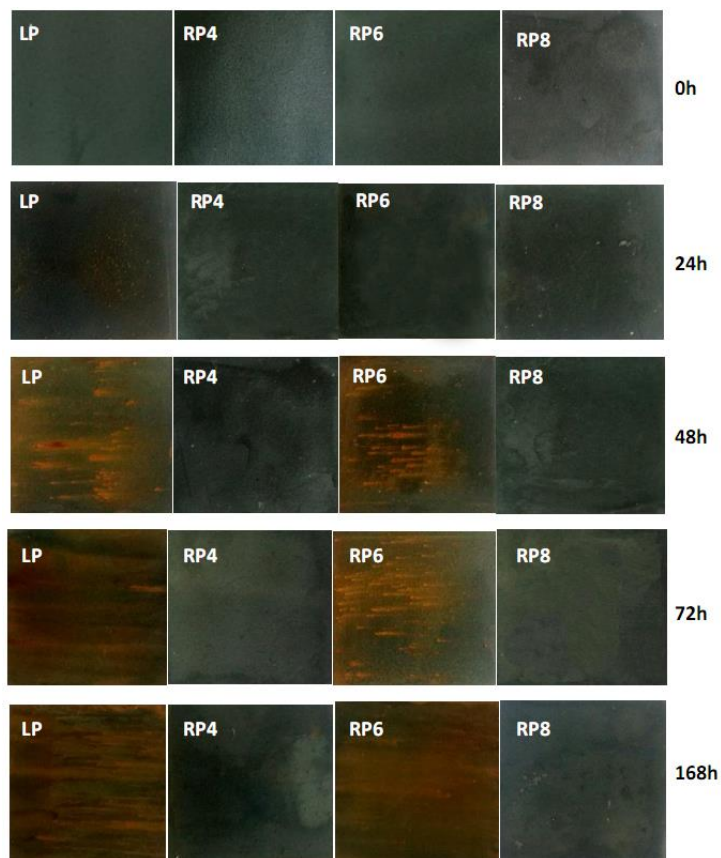
Figure 5. The surface image of the coating samples during the erosion-corrosion test.

4. CONCLUSIONS

Effect of heat treatment on microstructure and corrosion resistance of plasma sprayed Al_2O_3-TiO_2 coating sealed with aluminum phosphate is summarized as follows:

- Coatings after penetrating in the presence of ultrasonic excitation and heat-treated at 800 ^{o}C have the lowest porosity and the best corrosion and erosion-corrosion resistance in NaCl solution containing the causative agent of erosion in comparison with the samples heat-treated at 400 and 600 ^{o}C.

- The porosity treatment efficiency of the sealing with aluminum phosphate and heat treatment at 400 ^{o}C, 600 ^{o}C, and 800 ^{o}C for the Al_2O_3-40TiO_2 coating are 89.24 %, 80.05 %, and 95.29 %, respectively.

- The aluminum phosphate crystalline phases are detected on the surface of the samples including $Al(PO_3)_3$ (cubic), $Al(PO_3)_3$ (N), $Al_2P_6O_{18}$ (monoclinic), $AlPO_4$ (orthorhombic), and $AlPO_4$ (hexagonal). The presence of stable aluminum phosphate phases such as $Al(PO_3)_3$(cubic), $Al_2P_6O_{18}$(monoclinic), and $AlPO_4$(orthorhombic) after heat treatment at 800 ^{o}C has contributed to the improvement of corrosion resistance of the Al_2O_3-40TiO_2 coating.

Authors contribution: Tuan Nguyen Van: Writing – Original manuscript, Methodology, Supervision. Tuan Anh Nguyen: Formal analysis. Ha Pham Thi: Editing, Formal analysis. Ly Pham Thi: Writing, Editing, Formal analysis. Phuong Nguyen Thi: Editing, Formal analysis. Quy Le Thu: Review, Editing.

Statements of competing interest: The authors declare that they have no known competing financial interests or personal relationships that could have appeared to influence the work reported in this paper.

REFERENCES

1. Davis J. R. - Handbook of thermal spray technology. ASM International, Ohio, 2004.

2. Pawlowski L. - The science and engineering of thermal spray coatings, John Wiley & Sons Ltd, West Sussex, 2008.

3. Pinzón A. V., Urrego K. J., Hernández A. G., Ortiz M. R., and Galvis F. V. - Corrosion protection of carbon steel by alumina-titania ceramic coatings used for industrial applications, Ceram. Int. **44** (17) (2018) 21765-21773. https://doi.org/10.1016/j.ceramint.2018.08.273.

4. Tian W., Wang Y., Zhang T., and Yang Y. - Sliding wear and electrochemical corrosion behavior of plasma sprayed nanocomposite Al_2O_3–13%TiO_2 coatings, Mater Chem. Phys. **118** (2009) 37-45. https://doi.org/10.1016/j.matchemphys.2009.06.035.

5. Zavareh M. A., Sarhan A. A. D. M., Karimzadeh R., and Ramesh S. A. - Analysis of corrosion protection behavior of Al_2O_3-TiO_2 oxide ceramic coating on carbon steel pipes for petroleum industry, Ceram. Int. **44** (6) (2018) 5967-5975. https://doi.org/10.1016/j.ceramint.2017.12.175.

6. Vargas F., Ageorges H., Fournier P., Fauchais P., and López M.E. - Mechanical and tribological performance of Al_2O_3-TiO_2 coatings elaborated by flame and plasma spraying, Surf. Coat. Technol. **205** (4) (2010) 1132-1136. https://doi.org/10.1016/j.surfcoat.2010.07.061.

7. Wang L., Liu S., Gou J., Zhang Q., Zhou F., Wang Y., and Chu R. - Study on the wear resistance of graphene modified nanostructured Al$_2$O$_3$/TiO$_2$ coatings, Appl. Surf. Sci. **492** (2019) 272-279. https://doi.org/10.1016/j.apsusc.2019.06.102.

8. Verma R., Sharma S., Mukherjee B., Singh P., Islama A., Islam A., and Keshri A.K. - Microstructural, mechanical and marine water tribological properties of plasma-sprayed graphene nanoplatelets reinforced Al$_2$O$_3$- 40 wt% TiO$_2$ coating, J. Eur. Ceram. Soc. **42** (6) (2022) 2892-2904. https://doi.org/10.1016/j.jeurceramsoc.2022.02.014.

9. Knuuttila J., Sorsa P., Mäntylä T., Knuuttila J., and Sorsa P. - Sealing of thermal spray coatings by impregnation, J. Therm. Spray Technol. **8** (1999) 249-257. https://doi.org/10.1007/s11666-999-0002-2.

10. Leivo E. M., Vippola M. S., Sorsa P. P. A., Vuoristo P. M., and Mantyla T. A. - Wear and corrosion properties of plasma sprayed Al$_2$O$_3$ and Cr$_2$O$_3$ coatings sealed by aluminum phosphates, J. Therm. Spray Technol. **6** (1997) 205-210.

11. Ahmaniemi S., Vippola M., Vuoristo P., Mäntylä T., Buchmann M., and Gadow R. - Residual stresses in aluminium phosphate sealed plasma sprayed oxide coatings and their effect on abrasive wear, Wear **252** (7-8) (2002) 614-623. https://doi.org/10.1016/S0043-1648(02)00020-0.

12. Shao F., Yang K., Zhao H., Liu Ch., Wang L., and Tao S. - Effects of inorganic sealant and brief heat treatments on corrosion behavior of plasma sprayed Cr$_2$O$_3$–Al$_2$O$_3$ composite ceramic coatings, Surf. Coat. Technol. **276** (2015) 8-15. https://doi.org/10.1016/j.surfcoat.2015.06.045.

13. Nguyen V. T., Le T. Q., Pham T. H., Pham T. L. and Dinh T. M. T. - Influence of annealing temperature after sealing with aluminum phosphate on the corrosion resistance of thermal spray nicr20 alloy coating in sulfuric acid media, Vietnam J. Sci. Technol. **53** (1A) (2015) 36-43.

14. Nguyen V. T., Pham T. H., Pham T. L., Vo A. Q. , Dinh T. M. T., Le T. Q. and Pham D. R. - Study on the corrosive wear resistance of NiCr20 alloy coating impregnated by aluminum phosphate in acidic media, Vietnam J. Chem. **55** (1) (2017) 43-47. https://doi.org/10.15625/0866-7144.2017-00414.

15. Pham T. H., Pham T. L., Nguyen V. T. and Le T. Q. - Effects of aluminum phosphate sealant containing Al$_2$O$_3$ nanoparticles on the corrosion protective resistance ability of the Al$_2$O$_3$-TiO$_2$ plasma sprayed coating in NaCl media, Vietnam J. Chem. **55** (5E1,2) (2017) 49-53.

16. Nguyen V. T., Nguyen T. A., Pham T. H., Pham T. L., Nguyen T. P., Dao B. T., Trinh V. T., Vu D. and Le T. Q. - Sealing Treatment of Plasma-Sprayed Cr$_3$C$_2$-NiCr/Al$_2$O$_3$-TiO$_2$ Coating by Aluminum Phosphate Sealant Containing Al$_2$O$_3$ Nanoparticles, J. Therm. Spray Tech. **31** (2022) 269-281. https://doi.org/10.1007/s11666-021-01263-2.

17. Nguyen V. T, Nguyen T. A., Nguyen T. P., Pham T. H, Pham T. L., Ly Q. C., Hoang T. B. T., Vu D., and Le T. Quy. - Influence of ultrasonic sealing treatment with aluminum phosphate on properties of Al$_2$O$_3$-TiO$_2$ plasma sprayed ceramic coating, Proceedings of the International Thermal Spray Conference, Quebec City, 2021, pp 322-330.

18. Liu M. M., Hu H. X., and Zheng Y. G. - Effects of three sealing methods of aluminum phosphate sealant on corrosion resistance of the Fe-based amorphous coating, Surf. Coat. Technol. **309** (2017) 579-589. https://doi.org/10.1016/j.surfcoat.2016.12.033.

19. Niazi H., Yari S., Golestani-Fard F., Shahmiri M., Wang W., Alfantazi A., and Bayati R. - How deposition parameters affect corrosion behavior of TiO_2-Al_2O_3 nanocomposite coatings, Appl. Surf. Sci. **353** (2015) 1242-1252. https://doi.org/10.1016/ j.apsusc.2015.07.035.

20. Chen.D., He.L. and Shang.S, - Study on aluminum phosphate binder and related Al_2O_3-SiC ceramic coating, Mater. Sci. Eng., A. **348** (1-2) (2003) 29-35. https://doi.org/10.1016/ S0921-5093(02)00643-3.

21. He L., Chen D., and Shang S. - Fabrication and wear properties of Al_2O_3-SiC ceramic coatings using aluminum phosphate as binder, J. Mater. Sci. **39** (2004) 4887-4892. https://doi.org/10.1023/B%3AJMSC.0000035329.15101.77.

22. Kanta A. F., Planche M. P., and Montavon G. - Electrochemical Characterisations of Al_2O_3–13%TiO_2 Coated by Atmospheric Plasma Spray, Plasma Chem. Plasma Process **31** (2011) 867-877.

23. Shi P., Ng W. F., Wong M. H., and Cheng F. T. - Improvement of corrosion resistance of pure magnesium in Hanks' solution by microarc oxidation with sol–gel TiO_2 sealing, J. Alloys. Compd. **469** (1-2) (2009) 286-292. https://doi.org/10.1016/j.jallcom.2008.01.102.

24. Jones D. A. - On the so-called linear polarization method for measurement of corrosion rates, Corrosion **28** (5) (1972) 180-181. https://doi.org/10.5006/0010-9312-28.5.180.

25. Ozagem M. E. and Tribollet B. - Electrochemical impedance spectroscopy, The Electrochemical Society Series, John Wiley & Sons, New Jersey, 2008.

26. Zavareh M. A., Sarhan A. A. D. M., Zavareh P. A., Razak B. B. A., Basirun W. J., and Ismail M. B. C. - Development and protection evaluation of two new, advanced ceramic composite thermal spray coatings, Al_2O_3–40TiO_2 and Cr_3C_2–20NiCr on carbon steel petroleum oil piping, Ceram. Int. **42** (4) (2016) 5203-5210. https://doi.org/10.1016/ j.ceramint.2015.12.044.

27. BT-Lab & EC-Lab - Data Analysis and Processes, Version 11.00, 2015, 38.